Crystal structure of the GTPase domain of rat dynamin 1

Thomas F. Reubold*†, Susanne Eschenburg*†, Andreas Becker*‡, Marilyn Leonard§, Sandra L. Schmid§, Richard B. Vallee¶, F. Jon Kull‖, and Dietmar J. Manstein*,**††‡‡

*Abteilung Biophysik, Max-Planck-Institut für Medizinische Forschung, Jahnstrasse 29, D-69120 Heidelberg, Germany; §Department of Cell Biology, The Scripps Research Institute, La Jolla, California, CA 92037; ¶Department of Pathology and Cell Biology, College of Physicians and Surgeons, Columbia University, New York, NY 10032-3702; ‖Department of Chemistry, Dartmouth College, 6128 Burke Laboratory, Hanover, NH 03755; and **Institut für Biophysikalische Chemie, OE 4350, and ††Labor für Strukturanalyse, OE 8830, Medizinische Hochschule Hannover, 30623 Hannover, Germany

Communicated by Edwin W. Taylor, Northwestern University, Chicago, IL, August 1, 2005 (received for review April 11, 2005)

Here, we present the 1.9-Å crystal structure of the nucleotide-free GTPase domain of dynamin 1 from *Rattus norvegicus*. The structure corresponds to an extended form of the canonical GTPase fold observed in Ras proteins. Both nucleotide-binding switch motifs are well resolved, adopting conformations that closely resemble a GTP-bound state not previously observed for nucleotide-free GTPases. Two highly conserved arginines, Arg-66 and Arg-67, greatly restrict the mobility of switch I and are ideally positioned to relay information about the nucleotide state to other parts of the protein. Our results support a model in which switch I residue Arg-59 gates GTP binding in an assembly-dependent manner and the GTPase effector domain functions as an assembly-dependent GTPase activating protein in the fashion of RGS-type GAPs.

Dictyostelium | GTPase activating protein | GTPase effector domain | myosin | protein engineering

Members of the still expanding dynamin family of large GTPases are involved in a variety of different cellular processes, e.g., membrane severing events, vesicular trafficking, maintenance of mitochondrial morphology, and antiviral activity (reviewed in ref. 1). The best characterized member of the dynamin family is mammalian dynamin 1, an isoform exclusively expressed in brain and neuronal tissue, where it is a key component of the synaptic vesicle recycling machinery (2). Dynamin 1 has been shown to form ring-like assemblies around the necks of budding synaptic vesicles (3) and is necessary for the severing of newly formed vesicles from the presynaptic membrane (2). Impairment of GTP binding and/or hydrolysis adversely affects receptor-mediated endocytosis (4, 5), arresting the process at the stage of coated pits. *In vitro*, dynamin 1 is able to self-assemble under low-salt conditions into rings and helices (6) and to form helical arrays around microtubules and artificial lipid tubules (7, 8). Such self-assembly results in an up to 100-fold increase of GTPase activity (9, 10). Although the crucial role of dynamin 1 in endocytosis is established, there is an ongoing debate about the detailed function of dynamin 1 and its mode of action. Different mechanochemical models have been devised to explain how dynamin uses the chemical energy derived from GTP hydrolysis to drive vesicle fission by force generation (reviewed in ref. 11). Alternatively, it has been proposed that dynamin 1 acts as a regulatory GTPase that activates effector molecules depending on its nucleotide state (9).

Like all so-called genuine dynamins, dynamin 1 can be subdivided into five functionally distinct domains: the highly conserved N-terminal GTPase domain, the middle domain, the pleckstrin homology (PH) domain, the GTPase effector domain (GED), and the proline-rich domain (PRD). There is strong evidence that the GED, which interacts with the GTPase domain, the middle domain, and with itself, functions as an assembly-dependent GTPase-activating protein (GAP) that stimulates the GTPase activity of dynamin 1 as much as 100-fold (8–10). There are two principal modes of GAP action. For some GTPases, such as Ras (12), the very low basal rate of GTP hydrolysis can be stimulated up to 10,000-fold by GAPs, which introduce a missing catalytic residue, usually an arginine, into the active site of the GTPase. Other GTPases, such as the Gα-subunit of heterotrimeric G-proteins (13), already possess a catalytic arginine residue in their active site. In this case, the GAP molecule acts allosterically by positioning the intrinsic arginine residue for efficient catalysis and thus stimulates a relative high basal GTPase activity ≈100-fold (14). The high basal rate of GTPase activity of dynamin 1 of 1–2 min^{-1} (11) is reminiscent of that of Gα-subunits and suggests the presence of a catalytic residue within the GTPase domain itself.

We have solved the high-resolution x-ray structure of the GTPase domain of dynamin 1 from *Rattus norvegicus*. Based on this first model of a mammalian dynamin GTPase domain, we identified Arg-59 as suitably positioned to play a role as intrinsic stimulator of GTP hydrolysis. To test the role of Arg-59 in catalysis, we introduced the mutations Arg59Ala as well as Arg59Lys in full-length dynamin 1. Kinetic analysis revealed that the assembly-stimulated GTPase activity of the purified mutant proteins is not as drastically impaired as expected, which compromises the notion of Arg-59 as intrinsic arginine finger. We here discuss the implications of our findings for the mechanism of GTP hydrolysis by dynamin 1.

Materials and Methods

GTPase and Assembly Assays. Dynamin GTPase activity was measured at 37°C in GTPase assay buffer containing 20 mM Hepes (pH 7.5), 150 mM KCl, and 2 mM $MgCl_2$ by using a colorimetric malachite green assay to measure P_i release, exactly as described in ref. 15. Basal GTPase assays contained 0.5 μM dynamin, whereas assembly-stimulated GTPase assays contained 0.1 μM dynamin and 1 μg of PI4,5P_2-containing lipid nanotubules, prepared as described in refs. 8 and 15. The rate of inorganic phosphate (P_i) release (k_{obs}) was determined in the presence of 25, 50, 100, 200, 400, 800, and 1,200 μM GTP from at least five early time points during which P_i release was linear. Rates were plotted against [GTP] and curve fit by using the equation $k_{obs} = k_{cat}\,[GTP]/K_M + [GTP]$.

Protein Expression and Purification. Wild-type and mutant dynamins were expressed and purified from baculovirus-infected Tn5 cells as described in ref. 10. Residues 2–304 of the rat

Abbreviations: GAP, GTPase-activating protein; GED, GTPase effector domain.

Data deposition: The atomic coordinates and structure factors have been deposited in the Protein Data Bank, www.pdb.org (PDB ID code 2AKA).

†Present address: Abteilung Strukturelle Biologie, Max-Planck-Institut für Molekulare Physiologie, Otto-Hahn-Strasse 11, 44227 Dortmund, Germany.

‡Present address: Department of Medicinal Chemistry, University of Kansas, 4038 Malott Hall, Lawrence, KS 66045.

‡‡To whom correspondence should be addressed. E-mail: manstein@bpc.mh-hannover.de.

dynamin 1 GTPase domain were fused to the C terminus of the catalytic domain of *Dictyostelium* myosin II. The structure of the myosin part has been published elsewhere (16). The N-terminally His-tagged 120-kDa fusion protein was overproduced in *Dictyostelium* AX3-ORF$^+$ and purified essentially as described earlier for the myosin part alone (17). Cells were lysed with 0.5% (vol/vol) Triton X-100 in 20 cell volumes of buffer containing 50 mM Tris (pH 8.0), 2 mM EDTA, 0.2 mM EGTA, 2 mM dithiothreitol (DTT), 5 mM benzamidine, and protease inhibitors. The fusion protein was sedimented as actin rigor complex for 1 h at 30,000 $\times$ *g* and then resolubilized by homogenization in 2 cell volumes of extraction buffer containing 50 mM Hepes (*N*-2-hydroxyethylpiperazine-*N*′-2′-ethanesulfonic acid) (pH 7.3), 30 mM K-acetate, 300 mM NaCl, 14 mM Mg-acetate, 7 mM 2-mercaptoethanol, 10 mM ATP, 2 mM GTP, and protease inhibitors. After centrifugation for 20 min at 20,000 $\times$ *g*, the supernatant was applied to an XK16 column (Amersham Pharmacia) packed with Ni-NTA resin (Qiagen). The column was washed with three different buffers (50 mM Hepes, pH 7.3/300 mM K-acetate; 50 mM Hepes, pH 7.3/30 mM K-acetate; and 30 mM imidazole, pH 7.3). The fusion protein was eluted with a gradient from 50 to 500 mM imidazole over 5 column volumes. Peak fractions were pooled and dialyzed against storage buffer containing 50 mM Tris (pH 8.0), 1 mM $MgCl_2$, 5 mM DTT, and 3% (wt/vol) sucrose. The dialyzed fusion protein was further purified by size-exclusion chromatography using a Superdex 200 (Amersham Pharmacia) gel-filtration column equilibrated with storage buffer. Peak fractions were concentrated to 18 mg/ml by using 20 ml of Vivaspin concentration devices (Vivascience) with a cutoff of 50 kDa, subsequently flash-frozen in liquid nitrogen, and stored at −80°C.

Protein Crystallization. Crystals were grown by using the hanging-drop method at 4°C. The reservoir solution contained 11% (wt/vol) polyethylene glycol (PEG) 8000, 140 mM NaCl, 1 mM EGTA, 5 mM $MgCl_2$, 5 mM DTT, and 2% (vol/vol) 2-methyl-2,4-pentanediol (MPD). Two microliters of both reservoir solution and protein solution (18 mg/ml) were mixed, and crystals typically grew within 3–5 days to a size of ≈500 $\times$ 120 $\times$ 120 μm. For cryoprotection, crystals were transferred into a drop of 20 μl of reservoir solution with 13% (wt/vol) PEG 8000, then 20 μl of the same solution containing 50% (vol/vol) glycerol was added stepwise. A heavy-atom derivative was obtained by soaking a crystal for 12 h in reservoir solution with 13% (wt/vol) PEG 8000 containing 0.1 mM methyl mercury chloride. Cryoprotection was performed as described above, using cryoprotectant containing 0.1 mM of methyl mercury chloride. To ensure higher quality of the flash cooling, crystals were flash-frozen in liquid propane and transferred to liquid nitrogen for storage.

Data Collection and Processing. Native data were collected at 100 K on a charge-coupled device detector (Area Detector Systems) by using synchrotron radiation (λ = 0.939 Å) at beamline ID 14-4 in , France. A complete data set to 1.9-Å resolution was obtained by merging the data from two crystals. Heavy-atom data were collected to 2.3 Å from a single crystal at 100 K on a MAR345 image plate detector by using CuK_α radiation from a rotating anode (GX-18 generator, Elliott/Enraf-Nonius) operated at 35 kV and 50 mA. Native and derivative data were processed with XDS (18) and scaled with XSCALE (18).

Phasing, Model Building, and Refinement. The structure of the fusion protein was solved by the single isomorphous replacement with anomalous scattering (SIRAS) method, using a single mercury derivative. All calculations for phasing and refinement were performed with the program CNS (19). Building of the initial model and all manual adjustments during structure refinement were done with the program O (20). Refinement was performed by using data to highest resolution with no σ cutoff

Table 1. Data collection, structure solution, and refinement statistics

Data collection		
Crystal	Native	Derivative
Space group	$P2_12_12_1$	$P2_12_12_1$
Unit cell dimensions, Å	a = 57.4, b = 127.0, c = 160.8 $\alpha = \beta = \gamma = 90°$	a = 57.4, b = 127.0, c = 160.8 $\alpha = \beta = \gamma = 90°$
Molecules/asym. unit	1	1
Resolution range, Å	20–1.9 (2.0–1.9)	20–2.25 (2.3–2.25)
Measured reflections	1,215,184 (104,933)	512,629 (27,710)
Unique reflections	92,665 (12,446)	56,081 (3,447)
Completeness, %	99.1 (94.9)	98.5 (96.0)
R_{sym},* %	9.8 (17.1)	7.5 (27.7)
Phasing		
Resolution range, Å	15.0–2.30	
No. of sites	6	
Phasing power		
Isomorphous/anomalous	1.5/1.2	
Figure of merit	0.52	
Refinement		
Protein atoms	8,507	
Solvent molecules	754	
rmsd† bonds, Å	0.017	
rmsd angles	1.69	
R_{cryst},‡ %	18.5	
R_{free},§ %	22.4	

*$R_{sym} = 100 \times \Sigma_h\Sigma_i | I_{hi} - I_h | / \Sigma_{hi} I_{hi}$, where h are unique reflection indices.
†rmsd, root mean square deviation from ideal values.
‡$R_{cryst} = 100 \times \Sigma|F_{obs} - F_{model}|/\Sigma F_{obs}$, where F_{obs} and F_{model} are observed and calculated structure factor amplitudes.
§R_{free}: R_{cryst} calculated for randomly chosen reflections, which were excluded from the refinement (2.5% of the unique reflections).

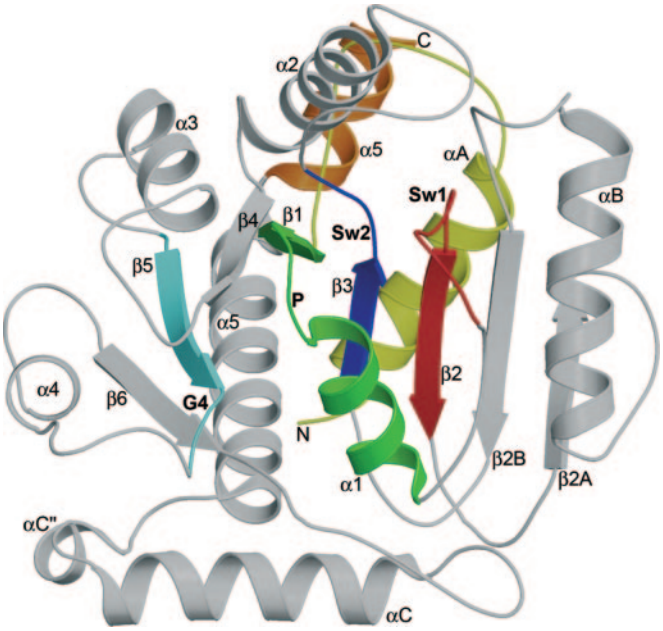

Fig. 1. Overall fold of the GTPase domain of dynamin 1. The core of the GTPase domain of dynamin 1 consists of an eight-stranded β-sheet containing six parallel strands and two antiparallel strands. The sheet is surrounded by seven α-helices and two single-turn helices. The nucleotide-binding motifs together with the attached secondary structure elements are colored as follows: green, P-loop; red, switch 1; blue, switch 2; turquoise, G4. The N- and C-terminal helices αA and α5 are highlighted in yellow and orange, respectively.

applied. Solvent molecules were automatically picked as implemented in CNS and checked manually.

Statistics of data collection, structure solution, and refinement are summarized in Table 1. The figures were prepared by using RASTER3D (21) in combination with MOLSCRIPT (22) or BOBSCRIPT (23).

Results and Discussion

Conformation of the Nucleotide-Binding Switch Motifs. The overall fold of the GTPase domain of dynamin 1 (Fig. 1) is an extension of the canonical GTPase fold observed in Ras proteins (24). Dynamin 1 contains in its GTPase domain the four guanine nucleotide binding motifs G1=^{38}*G*GQSA*GKS*^{45} (P-loop), G2=T^{65} (switch I), G3=^{136}*D*LP*G*^{139} (switch II) and G4=^{205}*TKLD*^{208}, which are conserved throughout all GTPases (highly conserved residues are italicized). As established by structural studies covering a wide variety of different GTPases (25), nucleotide binding is predominantly mediated via interactions of the P-loop with the α- and β-phosphates of the guanine nucleotide and of the G4 motif with the nucleotide base. Switch I and switch II usually undergo large conformational changes in the transition from the GTP state to the GDP state. Superposition of dynamin 1 with Ras-GTP (26) [Protein Data Bank (PDB) entry 5P21] and Ras-GDP (27) (PDB entry 1Q21) shows that, despite the absence of nucleotide, the active site conformation of dynamin 1 closely resembles Ras-GTP. Switch I and switch II are in conformations that other GTPases adopt only when GTP is bound or in the transition state (Fig. 2). In particular, the switch I threonine (Thr-65) is already rotated toward the nucleotide-binding site, and the switch II loop is arranged such that the main-chain nitrogen of Gly-139 would be almost in hydrogen-bonding distance with the γ-phosphate of a GTP molecule. Thr-65 and Gly-139 correspond to Thr-35 and Gly-60 in Ras (Fig. 2). Comparison of our structure with the GTP-bound structures of Ras (26) (PDB entry 5P21) and human

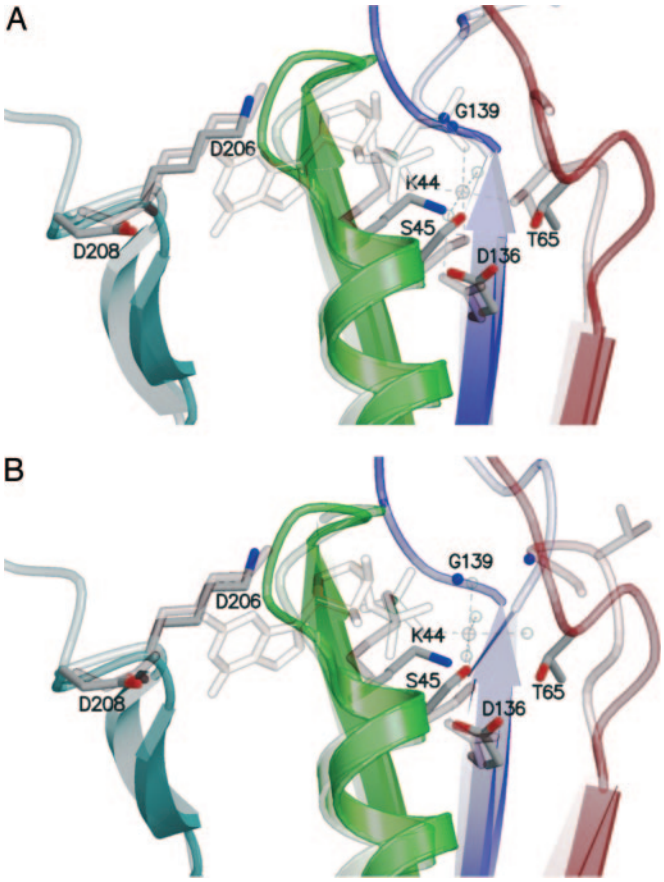

Fig. 2. Superposition of the nucleotide-binding sites of dynamin 1 and Ras. (*A*) Superposition with Ras-GTP (26) (PDB entry 5P21). (*B*) Superposition with Ras-GDP (27) (PDB entry 1Q21). The P-loop region of dynamin 1 is shown in green, switch I is in red, switch II is in blue, and G4 is in turquoise. Side chains involved in nucleotide binding are displayed as stick models with carbon atoms in gray, nitrogen atoms in blue, and oxygen atoms in red. The Ras structures are drawn semitransparent, and the respective nucleotides with magnesium ions and coordinating water molecules are fully transparent. The main-chain nitrogens of Gly-139 from dynamin 1 and of Gly-60 from Ras are shown as blue spheres. Residue numbering adheres to dynamin 1.

Guanylate Binding Protein 1 (28) (PDB entry 1F5N) suggests that switch I and switch II need to move by <2.5 Å and 1 Å from their positions in the nucleotide-free state to achieve full coordination of Mg^{2+}-GTP (Table 2). The GTP-state-like arrangement of switch II is stabilized through hydrogen bonds between the main chain at Met-140 and the main chain at Gly-38 and Gln-40 of the P-loop (Fig. 3). This β-sheet-like interaction restricts a rotation of the conserved Gly-139 around the tip of the preceding β-strand. Proper positioning of Gly-139 is essential for the formation of a hydrolysis-competent active site. Switch I is held in place through salt bridges from Arg-66 and Arg-67 to Asp-106 and Glu-104, respectively, located in helix αB (Fig. 3). Arg-66 and Arg-67 are highly conserved within the dynamin

Table 2. Distances between nucleotide binding motifs in dynamin 1, hGBP1, and Ras

	P-loop–switch I, Å	P-loop–switch II, Å	Switch I–switch II, Å
Dynamin 1	5.47	8.38	6.17
hGBP1	3.11	7.64	6.00
Ras	2.99	8.07	6.59

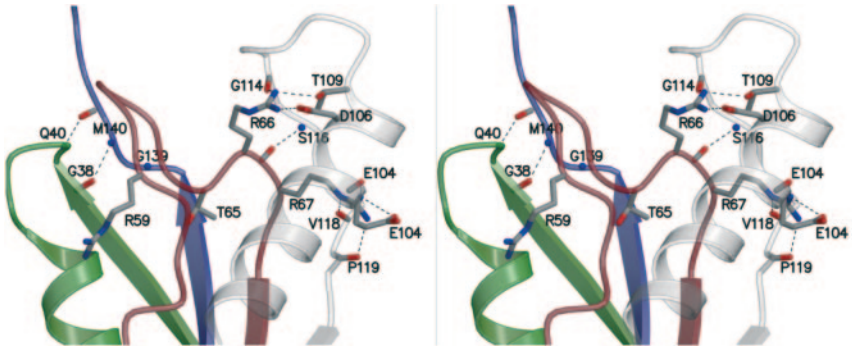

Fig. 3. Stabilization of the switch motifs (stereo view). P-loop and switch elements are colored as in Fig. 2, and αB and β2A are shown in light gray. Side chains and carbonyl groups are shown as stick models, and main-chain nitrogens are shown as blue spheres. Polar and ionic interactions are drawn as dotted lines.

family but not present in other GTPase families, and appear to communicate the shifts of switch I upon GTP binding and hydrolysis to helix αB.

Implications for the Mechanism of the Assembly-Dependent GTPase Stimulation. The increase of GTPase activity upon oligomerization of dynamin 1 to helical structures is thought to be induced by interaction between dynamin 1's GED and GTPase domains (9). Whether the GAP-function of the GED results from an allosteric action or from contributing one of its arginines to the catalytic center of the GTPase domain has been strongly debated (9, 10, 29). However, recent results favor a mechanism in which the GED functions by interacting with and stabilizing the switch II region, similar to RGS-type GAPs (14, 30). In agreement with these findings, our structure is not compatible with a mechanism involving an external arginine finger. A typical entrance route for a GAP arginine side chain is observed in Ras (31) and Rho (32) as the opening between the P-loop, the switch I loop, and the loop between β3 and α2 (Fig. 1). A considerably larger loop L8 and the side chain of conserved residue Gln-40 block a similar entrance route in dynamin 1. The only opening toward the nucleotide that would be sufficiently large to accommodate an external arginine side chain lies between the nucleotide and the switch I loop, approximately parallel to the longitudinal axis of the nucleotide. However, the expected shift of the switch I loop upon GTP binding is likely to obstruct this route. Alternatively, it has been suggested that four highly conserved arginine residues, at positions 54, 59, 66, and 67 within the switch I region, are directly involved in catalysis. Our structure shows that the α-carbon of Arg-54 is, with a distance of 17.4 Å to the β-γ bridging atom of the GTP-analogue from the superimposed Ras structure (26) (PDB entry 5P21), too remote to play a role in catalysis. Similarly, Arg-66 and Arg-67 can be excluded because reorientation of their guanidinium groups toward the nucleotide would drastically affect the orientation of the switch I threonine (Fig. 3). Because the side-chain interaction of Thr-65 is required for efficient GTP hydrolysis, movement of these arginines would severely compromise catalytic activity. However, the high degree of conservation of Arg-66 and Arg-67 suggests that limitation of the mobility of switch I is a specific and essential feature of dynamins. Arg-66 and Arg-67 may play an important role in communicating movements of switch I directly to αB and β2A and in restoring the relative position of Thr-65 once GTP hydrolysis is complete.

An active role of Arg-59 is suggested by the fact that it is located in approximately the same position as the catalytic Arg-174 of the α-subunit of a heterotrimeric G-protein (13) (Fig. 4). However, mutation Arg59Cys rescues the GTP binding defect displayed by *shi*^{ts2} mutants at 30°C. This mutation was identified in a genetic screen for *su*ppressors of *shi*^{ts2} (*sushi*) mutations (33).

To test whether Arg-59 plays a role in GTP binding or hydrolysis, we introduced mutations Arg59Ala or Arg59Lys into full-length dynamin 1 and purified the mutant proteins for kinetic analysis. Neither mutation strongly impaired dynamin's GTPase activity (Table 3). Arg59Ala and Arg59Lys retained 68% and 33% of basal GTPase activity relative to wild-type dynamin 1. The effect of the mutations on assembly-stimulated GTPase activity was only slightly stronger. The Arg59Ala and Arg59Lys mutants still retained 56% and 20% of residual lipid tubule-stimulated GTPase activity. A more pronounced difference between the two mutant proteins was observed for the K_M of the lipid tubule-stimulated GTPase activity. The Arg59Ala mutant showed a 12- and 7-fold reduced apparent affinity for GTP compared with Arg59Lys and wild type. The charge attraction between a positively charged side chain at position 59 and the phosphate moiety of the incoming GTP favors GTP binding significantly in the stimulated state. The observed K_M values for basal GTPase activity are generally larger and show much smaller differences for the mutant and wild-type proteins. In our structure, Arg-59 points away from the nucleotide-binding

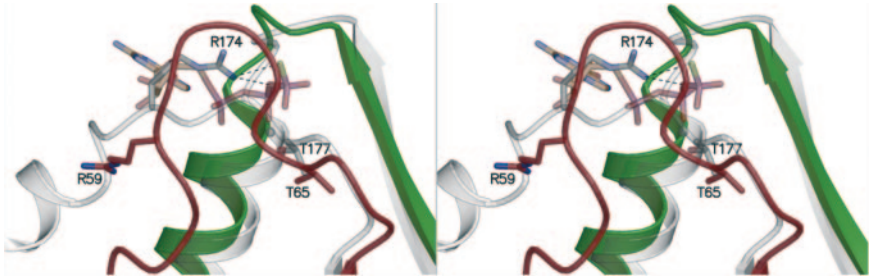

Fig. 4. Superposition of the switch I loop of dynamin 1 with that of the α-subunit of a heterotrimeric G protein (13) ($G_{t\alpha}$; PDB entry 1TND) (stereo view). The P-loop region of dynamin 1 is colored in green, and switch I is in red. Secondary structure elements and side chains of $G_{t\alpha}$ are shown in gray. The GTP-analogue GTPγS of $G_{t\alpha}$ is drawn semitransparent. The interaction of the catalytically active Arg-174 of $G_{t\alpha}$ with the γ-phosphate moiety is designated by dotted lines.

Table 3. Kinetic parameters for basal and assembly-stimulated GTPase activity of wild-type and mutant dynamins measured at 37°C

	Basal GTPase activity		Lipid tubule-stimulated GTPase activity	
Dynamin	k_{cat}, min^{-1}	K_M, μM GTP	k_{cat}, min^{-1}	K_M, μM GTP
WT	1.45 ± 0.026	46.0 ± 0.40	123.7 ± 7.9	30.0 ± 10.0
R59K	0.474 ± 0.054	96.0 ± 4.1	25.5 ± 0.97	18.0 ± 5.0
R59A	0.980 ± 0.060	241.0 ± 43.0	69.7 ± 3.6	211.0 ± 33.0

Values are averages ± SD from three independent experiments.

site, but rotation around the main chain, in concert with the expected shift of switch I upon nucleotide binding, can bring the guanidinium group of Arg-59 close to the γ-phosphate (Fig. 3). Transposition of the arginine side chain toward the nucleotide phosphates is facilitated by the close proximity of Gly-60 and Gly-62, which ensures a high degree of rotational freedom in this region. The observed increase in the apparent GTP affinity upon stimulation with lipid tubules suggests that dynamin assembly may act as a trigger that shifts the equilibrium of conformers to an orientation in which the Arg-59 side chain points toward the nucleotide facilitating GTP binding by charge attraction. In the absence of a positive side chain at position 59, no change in the apparent GTP affinity between basal and stimulated assay conditions is expected, as is indeed observed for Arg59Ala.

Recent studies suggest that the GED does not function as a classical GAP but rather in the fashion of RGS-type GAPs in ordering and optimally positioning catalytic residues already present in the GTPase domain (10, 30). As previously suggested, the hydrophobic groove formed by the N- and C-terminal helices αA and α5 of the *Dictyostelium* dynamin A GTPase domain could mediate the interactions with the GED (34). In dynamin A, which was also crystallized as a fusion with the *Dictyostelium* myosin II motor domain, helices αA and α5 interact with each other through hydrophobic residues that are arranged in a zipper-like fashion, and the helix emerging from the myosin motor domain docks into the resulting groove. A tighter interaction is now observed for the corresponding helices of the dynamin 1 GTPase domain. Although the αA helices of dynamin 1 and dynamin A superimpose well, helix α5 of dynamin 1 is more kinked at Pro-294. This increased kink leads to a parallel arrangement of the two groove helices in dynamin 1 (Fig. 5) and a shorter hydrophobic interaction distance toward the C-terminal end of helix α5. For instance, the distance between Phe-20 of helix αA and Leu-304 of helix α5 is 3.7 Å in dynamin 1, whereas the corresponding distance is 4.6 Å in the case of dynamin A. The C-terminal helix of the myosin motor domain docks almost parallel to both groove helices in the case of dynamin 1 but is tilted by ≈30° with respect to helix αA in the dynamin A fusion. The interaction of the groove formed by αA and α5 with a partially hydrophobic helix in two independent crystal structures corroborates the suggestion of Niemann *et al.* (34), that the groove acts as a docking site for the GED, which indeed provides several amphiphatic helical stretches (35).

The following observations indicate that dynamin fusion protein structures represent biologically significant states. The structures of the myosin motor domains obtained for the dynamin 1 and dynamin A fusions show large conformational differences (16), but very similar structures were obtained for the myosin motor domain constructs alone (36, 37). The crystal packing is completely different for the dynamin 1 and dynamin A fusions; therefore, it is unlikely that the interaction between the myosin helix and the hydrophobic groove is a crystallization artifact. Finally, both fusion constructs move actin filaments in an *in vitro* motility assay, which indicates that the dynamin GTPase domains is not sterically constrained and can rotate during the myosin ATPase cycle and act as a lever arm similar to the native myosin neck region.

In conclusion, our results lend support to a mechanism in which the GED functions as an assembly-dependent GAP in the fashion of RGS-type GAPs (14, 38). Arg-59 does not act as an arginine finger but appears to gate GTP binding in an assembly-dependent manner. How exactly the GED is involved in assembly-stimulated GTPase, tetramerization, and higher-order assembly of dynamin remains to be elucidated and will require detailed structural information about the full-length protein.

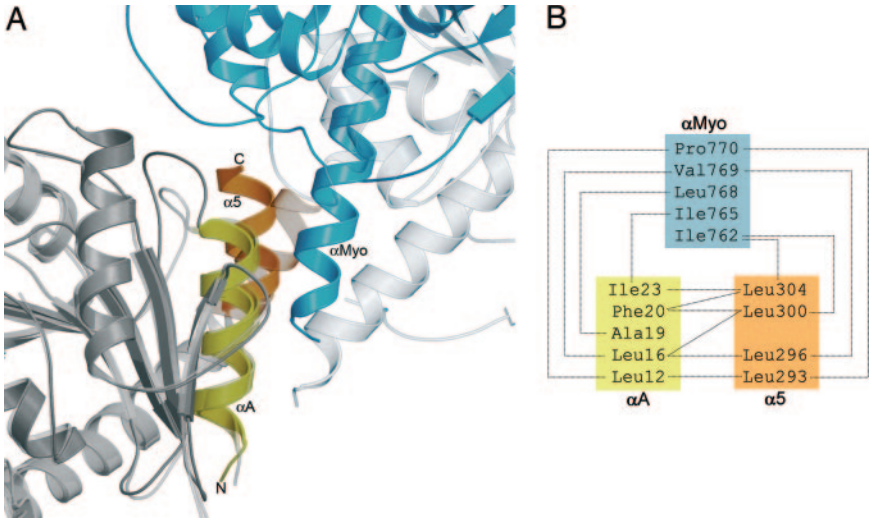

Fig. 5. Docking of the C-terminal myosin helix into the hydrophobic groove of dynamin. (*A*) The structure of the dynamin 1–myosin fusion as solid cartoon with the dynamin 1 GTPase domain drawn in dark gray, the groove helices αA and α5 in yellow and orange, respectively, and the myosin motor domain in blue. The structure of the dynamin A fusion is superimposed in transparent gray. Although the dynamin domains align well, the myosin motor domains adopt different conformations in the dynamin 1 and dynamin A fusion structures. (B) Schematic representation of the hydrophobic interactions (solid lines between the respective amino acid partners) between helices αA (yellow box) and α5 (orange box) and the C-terminal myosin helix (blue box).

We thank S. Zimmermann for excellent technical assistance and Kenneth C. Holmes for helpful discussions and continuous support. This work was supported by Deutsche Forschungsgemeinschaft Grants Ku1288/2-2 (to F.J.K.), GM47434 (to R.B.V.), and Ma1081/8-1 (to D.J.M.).

1. Danino, D. & Hinshaw, J. E. (2001) *Curr. Opin. Cell Biol.* **13,** 454–460.
2. Hinshaw, J. E. (2000) *Annu. Rev. Cell Dev. Biol.* **16,** 483–519.
3. Takei, K., McPherson, P. S., Schmid, S. L. & De Camilli, P. (1995) *Nature* **374,** 186–190.
4. Herskovits, J. S., Burgess, C. C., Obar, R. A. & Vallee, R. B. (1993) *J. Cell Biol.* **122,** 565–578.
5. van der Bliek, A. M., Redelmeier, T. E., Damke, H., Tisdale, E. J., Meyerowitz, E. M. & Schmid, S. L. (1993) *J. Cell Biol.* **122,** 553–563.
6. Hinshaw, J. E. & Schmid, S. L. (1995) *Nature* **374,** 190–192.
7. Shpetner, H. S. & Vallee, R. B. (1989) *Cell* **59,** 421–432.
8. Stowell, M. H., Marks, B., Wigge, P. & McMahon, H. T. (1999) *Nat. Cell Biol.* **1,** 27–32.
9. Sever, S., Muhlberg, A. B. & Schmid, S. L. (1999) *Nature* **398,** 481–486.
10. Song, B. D., Yarar, D. & Schmid, S. L. (2004) *Mol. Biol. Cell* **15,** 2243–2252.
11. Sever, S., Damke, H. & Schmid, S. L. (2000) *Traffic* **1,** 385–392.
12. Gideon, P., John, J., Frech, M., Lautwein, A., Clark, R., Scheffler, J. E. & Wittinghofer, A. (1992) *Mol. Cell. Biol.* **12,** 2050–2056.
13. Noel, J. P., Hamm, H. E. & Sigler, P. B. (1993) *Nature* **366,** 654–663.
14. Ross, E. M. & Wilkie, T. M. (2000) *Annu. Rev. Biochem.* **69,** 795–827.
15. Song, B. D. & Schmid, S. L. (2003) *Biochemistry* **42,** 1369–1376.
16. Reubold, T. F., Eschenburg, S., Becker, A., Kull, F. J. & Manstein, D. J. (2003) *Nat. Struct. Biol.* **10,** 826–830.
17. Manstein, D. J. & Hunt, D. M. (1995) *J. Muscle Res. Cell Motil.* **16,** 325–332.
18. Kabsch, W. (1993) *J. Appl. Crystallogr.* **26,** 795–800.
19. Brunger, A. T., Adams, P. D., Clore, G. M., DeLano, W. L., Gros, P., Grosse-Kunstleve, R. W., Jiang, J. S., Kuszewski, J., Nilges, M., Pannu, N. S., *et al.* (1998) *Acta Crystallogr. D* **54,** 905–921.
20. Jones, T. A., Zou, J. Y., Cowan, S. W. & Kjeldgaard, M. (1991) *Acta Crystallogr. A* **47,** 110–119.
21. Merritt, E. A. & Bacon, D. J. (1997) *Methods Enzymol.* **277,** 505–524.
22. Kraulis, P. J. (1991) *J. Appl. Crystallogr.* **24,** 946–950.
23. Esnouf, R. M. (1997) *J. Mol. Graphics Model.* **2,** 132–134.
24. Kjeldgaard, M., Nyborg, J. & Clark, B. F. (1996) *FASEB J.* **10,** 1347–1368.
25. Vetter, I. R. & Wittinghofer, A. (2001) *Science* **294,** 1299–1304.
26. Pai, E. F., Kabsch, W., Krengel, U., Holmes, K. C., John, J. & Wittinghofer, A. (1989) *Nature* **341,** 209–214.
27. Tong, L. A., de Vos, A. M., Milburn, M. V. & Kim, S. H. (1991) *J. Mol. Biol.* **217,** 503–516.
28. Prakash, B., Renault, L., Praefcke, G. J., Herrmann, C. & Wittinghofer, A. (2000) *EMBO J.* **19,** 4555–4564.
29. Marks, B., Stowell, M. H., Vallis, Y., Mills, I. G., Gibson, A., Hopkins, C. R. & McMahon, H. T. (2001) *Nature* **410,** 231–235.
30. Narayanan, R., Leonard, M., Song, B. D., Schmid, S. L. & Ramaswami, M. (2005) *J. Cell Biol.* **169,** 117–126.
31. Scheffzek, K., Ahmadian, M. R., Kabsch, W., Wiesmüller, L., Lautwein, A., Schmitz, F. & Wittinghofer, A. (1997) *Science* **277,** 333–338.
32. Rittinger, K., Walker, P. A., Eccleston, J. F., Smerdon, S. J. & Gamblin, S. J. (1997) *Nature* **389,** 758–762.
33. Ramaswami, M., Rao, S., van der Bliek, A., Kelly, R. B. & Krishnan, K. S. (1993) *J. Neurogenet.* **9,** 73–87.
34. Niemann, H. H., Knetsch, M. L., Scherer, A., Manstein, D. J. & Kull, F. J. (2001) *EMBO J.* **20,** 5813–5821.
35. Okamoto, P. M., Tripet, B., Litowski, J., Hodges, R. S. & Vallee, R. B. (1999) *J. Biol. Chem.* **274,** 10277–10286.
36. Coureux, P. D., Sweeney, H. L. & Houdusse, A. (2004) *EMBO J.* **23,** 4527–4537.
37. Gulick, A. M., Bauer, C. B., Thoden, J. B. & Rayment, I. (1997) *Biochemistry* **36,** 11619–11628.
38. Scheffzek, K., Ahmadian, M. R. & Wittinghofer, A. (1998) *Trends Biochem. Sci.* **23,** 257–262.